Article:
Huang, L., Li, Y., Kontziampasis, D. et al. (2026) Fabrication of polymeric nanostructures with high aspect ratio for cell differentiation. Colloids and Surfaces B: Biointerfaces, 266. 115797. ISSN: 0927-7765

https://doi.org/10.1016/j.colsurfb.2026.115797

Fabrication of polymeric nanostructures with high aspect ratio for cell differentiation

Lei Huang[1], *Yuan Li*[1], *Dimitrios Kontziampasis*[3], *Wangqing Wu*[1,2], *Bingyan Jiang*[1,2], *Mingyong Zhou*[1,2*]

1. College of Mechanical and Electrical Engineering, Central South University, Changsha 410083, P. R. China

2. State Key Laboratory of Precision Manufacturing for Extreme Service Performance, Central South University, Changsha 410083, P. R. China

3. Institute of Medical and Biological Engineering, School of Mechanical Engineering, Faculty of Science and Engineering, University of Leeds, LS2 9JT, Leeds, Yorkshire, UK

* Corresponding author: Mingyong Zhou; Email: mingyong.zhou1989@csu.edu.cn

Abstract

The regulation of stem cell fate by using the physicochemical signals is a hot research topic in tissue engineering. Compared to biochemical growth factors, mechanical stimulation such as surface nanostructures can remodel the microenvironment in which cells are located to via their own physical properties. To fabricate bioresorbable nanostructures with an optimal design for cell differentiation, a robust and versatile process chain needs to be developed. In this work, a process chain combining self-assembled mold inserts and injection molding was proposed to fabricate nanopillars with different aspect ratios as the substrates for cell culture. Herein, the optimal parameters affecting the anodic oxidation process for mold inserts and the injection molding process for nanopillar were investigated. The injection-molded nanopillars were then applied to the differentiation experiments of bone marrow mesenchymal stem cells (BMSCs). The results showed that nanopillar structures with different aspect ratios were precisely fabricated through the process chain. Nanopillars had a significant osteogenic differentiation inducing effect on BMSCs, and the inducing effect became stronger with the increase in the aspect ratio. Compared with the addition of osteogenic inducers, nanopillar substrates exhibited a better effect in inducing differentiation and provided an alternative protocol for differentiation

induction.

Keywords: Polymers; High aspect ratio; Nanopillar arrays; AAO templates; Injection molding; Stem cell culture and differentiation

1. Introduction

Nanofabrication is an established technology with a plethora of life science related applications ranging from biosensing detection[1,2], optomechanical analysis[3,4], antibacterial and infiltration analysis[5,6], and bioengineering[7,8]. As a highly interdisciplinary research field, tissue engineering utilizes the self-replication ability and differentiation potential of stem cells[9,10] as fundamental elements to repair, replace, and regenerate defective tissues[11]. Cell culture is one of the most fundamental technologies in the fields of biology and medicine[12]. By using nanostructures to construct a cell culture method that is closer to the physiological environment of the body, it can provide cells with a biomimetic environment for growth and information transmission[13,14]. Current studies have demonstrated that nanomaterials can regulate the biological behaviors of bone-related cells, and thus be applied to induce osteogenic differentiation and treat postmenopausal osteoporosis[15,16]. Moreover, compared with biochemical growth factors, nanostructures have almost no potential side effects on the human body, and have good biological stability and health safety[17–21].

Nowadays, with the development of nanostructure processing technologies such as nano-assembly[22], etching, plasma nanofabrication[23], laser modification[24] and nanoimprinting[25], the preparation methods of ordered nanostructures have gradually matured. Most fabrication technologies for nanostructures are difficult to enable mass production; therefore, it is necessary to develop a robust and versatile process chain. The combination of the self-assembled anodic aluminum oxide (AAO) and the mass production advantages of injection molding can greatly overcome the challenges and reduce the high costs associated with nanostructure fabrication. The research on nano injection molding technology mainly focuses on process control, among which increasing the mold temperature is one of the most effective methods to improve the molding quality of nanostructures, especially for high aspect

ratio nanopillars[26–28]. Therefore, it is necessary to explore the process parameters related to self-assembled AAO and injection molding to meet the applications of nanopillars.

Due to their excellent biocompatibility, polymeric substrates with surface nanostructures are often used to simulate microenvironments for biological experiments. In addition, polymeric materials have shown excellent processability, temperature resistance, and high elastic modulus, rendering them as ideal candidates for being used as substrates where one can fabricate nanostructures on their surface. The physical clues, particularly the nano-morphology of substrates, play a crucial role in guiding stem cell differentiation[29–31]. Many scholars have attempted to simulate the cellular microenvironment for different types of cells, such as immune cells[32], tumor cells[33], nerve cells[34], heart cells[35], bone cells[36] and stem cells.[37–41] Numerous types of stem cells are commonly used in tissue engineering,which include embryonic stem cells, mesenchymal stem cells, neural stem cells, and hematopoietic stem cells[42]. Among them, osteogenic differentiation of stem cells is one of the most widely studied fields. Currently, research on the effect of nanopillar structure size on osteogenic differentiation mainly discusses the influence of height in the low aspect ratio range of 100-500 nm[43], with scarce studies investigating the effects of polymeric nanopillars with higher aspect ratios on the fate regulation and cell differentiation needs[44].

Based on the application demand for inducing the differentiation of bone marrow mesenchymal stem cells (BMSCs), a process chain combining self-assembled AAO templates as the mold inserts and injection molding was proposed to fabricate surface nanopillar structures with different aspect ratios as the substrates for cell culture and osteogenic differentiation, as shown in Fig.1. Compared with previously reported nanostructure fabrication techniques such as nanoimprinting, 3D printing and soft lithography, the injection molding strategy proposed herein enables high-throughput and reproducible fabrication of nanopillar substrates for cell culture, with reduced manufacturing costs and promising industrial translation potential. Moreover, based on the established regulatory mechanism of substrate surface topography in modulating stem cell fate[17,31], that nanopillars facilitate stem cell osteogenic differentiation via mechanical stimulation and the YEP-related signaling pathways[39,45], the injection molding experiments of nanopillars with different aspect ratios were systematically conducted. The influence of process parameters on the anodic oxidation

and injection molding was explored to improve the fabrication quality of nanopillars. Based on this, the height and diameter of nanopillars can be adjusted over a large range, resulting in structures with different aspect ratios. When the BMSCs were cultured on the substrate surface, their activity, proliferation, cell morphology, differentiation-related proteins were analyzed at different periods to explore the effect of different aspect ratio nanopillars structures on the osteogenic differentiation of BMSCs.

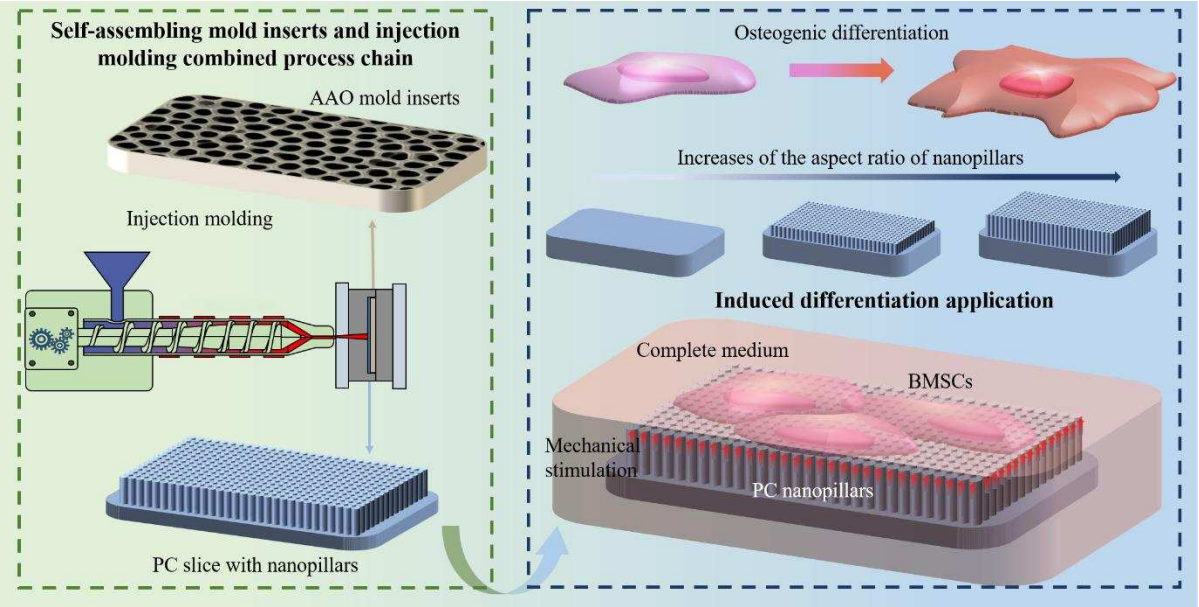

Figure 1. Schematic diagram showing the PC substrate with nanopillars by injection molding based on the AAO mold insert to induce osteogenic differentiation of BMSCs. By adjusting the preparation process of AAO mold inserts and the injection molding process of polycarbonate (PC), the formation of nanopillar arrays with different aspect ratios was achieved. Based on the results of cell culture and biomarker analysis, the effect of nanopillars on osteogenic differentiation of BMSCs was characterized.

2. Experimental Section

2.1. Preparation of AAO mold insert

The preparation of AAO mold insert includes two steps. One is the electrolytic polishing to reduce the surface defects, and the other is anodic oxidation to generate nanopore structures. In these experiments, high-purity aluminum sheets with a thickness of 1 mm were used as the anode and high-purity graphite was used as the cathode for the electrolytic reaction. The experimental setup is shown in Fig.S1.

Initially, 68% perchloric acid (Top Journal Agent, China) and anhydrous ethanol (HengXing Chemical Reagent, China) was mixed in a volume ratio of 1:6.The aluminum sheet

was placed into the mixture, with a 15 V DC power (WANPTEK, China) for 25 min to accomplish the polishing process. Throughout the entire process, the electrolyte temperature was maintained at 10 ℃. After the polished aluminum sheet was cleaned, the AAO template with nanopore structure was fabricated by the secondary anodic oxidation process under constant voltage. The phosphoric acid (Yien Chemical Reagent, China, ≥85wt.%) solution was used as the electrolyte, which was controlled at 0~4 ℃ through a circulating water bath. A mixed solution of 30 g/L chromium trioxide (Macklin Biochemical, China) and 50 ml/L phosphoric acid was then prepared to remove the oxide layer at 75 ℃ for 30 min. The second anodizing process was performed under the same experimental conditions after removing, cleaning, and drying the anodic oxide film. To prepare structures with different aspect ratios for biological applications, AAO mold inserts with highly ordered and adjustable depths were prepared for injection molding by adjusting the anodizing parameters as shown in Table S1.

2.2. Fabrication of surface nanostructures by injection molding

An injection mold with a size of 126 mm × 126 mm was designed where the mold insert can be quickly installed by utilizing a pressing plate and a cover plate between the inserts of the moving and fixed halves. The method of electrical heating and oil cooling was applied to realize the vario-thermal technology. The prepared AAO mold insert was cut into a size of 25 × 25 mm, and then fixed in the mold cavity on the injection molding machine (Sodick LD05EH2, Japan). The PC (Iupilon® S-3001R, China) was used as the molding material to fabricate nanopillar substrates, due to its good biocompatibility. The effects of process parameters on the structural evolution of nanopillars were studied, in order to control the aspect ratio of injection-molded nanopillars. To ensure accuracy of experimental data, benchmark parameters were set as mold temperature of 140 ℃, injection speed of 18 cm^3/s, holding pressure of 110 MPa, holding time of 5 s, melt temperature of 290 ℃, and cooling time of 120 s. The investigation of process parameter effects was carried out by changing a single factor separately. The initial values of each process parameter are shown in Table S2.

2.3. Characterization of the nanostructures

The prepared AAO mold insert was characterized by a field emission scanning electron microscopy (FE-SEM, TESCNA MIRA 3, Czech Republic). The contact angle gonio meter

(JC-2000D, POWEREACH, China) was used to analyze the surface contact angle of injection-molded parts to characterize their wettability. After spraying gold on the parts using a spray gold analyzer (Leica, EM ACE200, Germany), the microstructure of the injection-molded nanopillar was observed under the SEM.

2.4. Cell Culture and Cell Viability

2.4.1. Cell Culture

The BMSCs used in this work were extracted from Sprague-Dawley rats and purchased from the Stem Cell Bank of the Chinese Academy of Sciences (CAS). The purchased BMSCs were cultured in a 37 °C incubator containing 5% CO_2. The cells were put in a growth culture medium containing DMEM medium (Gibco, USA), 10% fetal bovine serum (Gibco, USA), 1% penicillin-streptomycin (Gibco, USA).

2.4.2. Cell Viability Assay

The live/dead cell staining kit (BB-4126, BestBio, China) was used to visually evaluate the survival status of cells on matrices with different aspect ratios of nanopillars. Four groups of sterilized substrate samples were placed in a well plate, and logarithmic growth length BMSCs were taken for cell counting and cell concentration adjustment. The samples were seeded into a 6-well plate at 2×10^5/well and cultured for 24 h and 48 h, respectively. The staining solution was prepared according to the instructions of the viability staining kit and stained in a 5% CO_2, 37 °C constant temperature incubator for 20 min. The fluorescence was then captured using a confocal laser scanning microscope (Olympus FV1200, Japan).

2.4.3. CCK-8 Cell Proliferation Assay

The CCK-8 (IV08-100, Invigentech, USA) was used to quantitatively evaluate cell proliferation and explore the survival, proliferation, and diffusion of stem cells. The sample was placed in a well plate, taking the logarithmic growth length BMSCs for cell counting, by adjusting the cell concentration, and inoculating them into a 6-well plate at 1×10^5/well. After 1, 3, and 6 days of culture, the supernatant was discarded and washed with PBS. Culture medium containing 10% CCK-8 reagent was added at 100 μL/well and incubated in a 5% CO_2, 37 °C constant temperature incubator for 2 h. A 100 μL solution was taken into a 96-well plate

and the absorbance was detected at 450 nm by a microplate reader (SPARK 10M, TECAN, Switzerland).

2.5. Cell Staining for BMSCs Differentiation

2.5.1. Immunofluorescence Staining

The F-actin is the main component of the cytoskeleton, providing mechanical support for cells, which can be stained red by Rhodamine Phalloidin to observe cell migration morphology [46,47]. The expression of Vinculin can indicate the cell's adhesion, migration ability, and response to the microenvironment, which can be stained green by Goal Anti Rabbit IgG (H+L) FITC conjugated. The nucleus DNA can be stained blue by DAPI solution, which is commonly used for nuclear staining. In this study, four groups of sterilized substrate samples with different aspect ratios were placed in a well plate, and logarithmic growth length BMSCs were taken for cell counting. The cell concentration was adjusted and seeded into a 6-well plate at 2×10^5/well. After 48 h of cultivation, the supernatant was discarded and washed with PBS. Subsequently, a 4% paraformaldehyde (SL1830, Coolaber, China) was added for cell fixation. At next step the cell was washed three times with PBS, soaked in 0.5% Triton-X-100 reagent (T8200, Solarbio, China) for 5 min to change the selective permeability of the cell membrane. Thereafter, it was blocked with 5% BSA (bovine serum albumin) (164210-50, Procell, China) for 1 h and washed once with PBS, and then added Vinculin primary antibody (26520-1-AP, Proteintech Group, China) working solution and incubated overnight at 4 ℃. Next, Replaced the fluorescent secondary antibody labeled with FITC (S0008, Affinity, China), and incubated at room temperature for 1 hour. Finally, added a mixture of Rhodamine-Phalloidin (CA1610, Solarbio, China) and DAPI(4', 6-diamidino-2-phenylindole) staining (C0060, Solarbio, China), and incubated at room temperature for 10 min.

2.5.2. Alkaline phosphatase (ALP) Staining

The cultivation operation of BMSCs was the same as described in the previous section. Discarded the medium, and added 4% paraformaldehyde for cell fixation. After staining according to the instructions in the ALP kit (C3250S, Biyotime, China), the ALP was observed under a fluorescence microscope (TI2-U, Nikon, Japan). At the same time, the cells were washed with PBS, and added 300 μL/well of Western and IP cell lysis buffer. By collecting the

lysate, the absorbance was measured at 405 nm using a microplate reader (SPARK 10M, TECAN, Switzerland) according to the instructions of the ALP detection kit (P0321, Biyotime, China). The control group was cultured with BMSCs in normal medium, while the model group was cultured with commercial osteogenic differentiation medium for BMSCs (PD-003, Procell, China) which contains DMEM medium, FBS, dexamethasone, β-sodium glycerophosphate, ascorbic acid and transferrin. The 6-well plate material used for cell culture in the experiment was polypropylene (PP), and alkaline phosphatase (ALP) staining and quantitative detection were performed at day 7 and day 14, respectively.

In this study, two materials, PP and PC, were adopted as cell culture substrates. To exclude the influence of substrate material differences on the osteogenic differentiation of BMSCs, we first compared the experimental outcomes between the control group and the model group, and confirmed that the PP substrate had no notable impact on BMSC osteogenic differentiation. Afterwards, the model group was defined as the positive control and the control group as the negative control, so as to further investigate the regulatory effects of PC substrates with different aspect ratios on BMSC osteogenic differentiation.

2.5.3. Calcium Nodule Staining

The cultivation operation of BMSCs was the same as described in the previous section. Taken the test after 21 days of cultivation, discarded the culture medium, fixed the BMSCs with 4% paraformaldehyde, washed them once with PBS after fixation, and then stained with Alizarin Red (C0148S, Biyotime, China) for about 10 mins. Washed it 1-2 times with distilled water, and then the calcium nodule staining by Alizarin Red S (ARS) were observed under the microscope. Images of ARS-stained calcium nodules were processed using ImageJ software, and the ARS staining area under different experimental conditions was quantified. With the model group as the reference, all data were normalized to realize the quantitative analysis of ARS staining results.

3. Results and Discussion

3.1. Surface nanostructures on AAO mold inserts

In this study, the preparation of nanopillar substrates with different aspect ratios was achieved by changing the depth of nanopores in the AAO mold insert. The surface order degree

at 135 V and 165 V was lower than that prepared at 195 V, as shown in Fig. 2(a-c). Hexagonal structures from the surface can be observed. From the cross-section of the AAO, it can be observed that as the applied voltage increased, the growth rate and the final depth of nanopore also increased significantly, as shown in Fig. 2(e-f). The concentration of phosphoric acid was adjusted in the electrolyte to obtain appropriate process parameters. When the concentration was increased to 0.2 M and 0.3 M, the uniformity of nanopores diameter distribution was significantly better than that of 0.1 M (over 72.3% of the nanopores have a diameter of approximately 200 ± 20nm), and the nanopore surface exhibited a standard hexagonal structure, as shown in Fig. 2(g-i). The growth rate of nanopores was slower at the concentration of 0.1 M, while the growth rate of nanopores was basically the same at concentrations of 0.2 M and 0.3 M, as shown in Fig. 2(j-l). For this reason, it was determined to use 195 V and 0.2 M phosphoric acid concentration for the study.

The changes in current density during the primary and secondary anodizing processes were analyzed, as shown in Fig. 2(m) and 2(n). It was shown that at the moment of connecting to a high voltage electric field, the current density reached its maximum, and then gradually decreased. The current density of secondary anodizing was more stable than that of primary anodizing, basically stable at around 2500 A/cm^2. In order to maintain the stability of the nanopillar diameter, the reaming process was applied to keep the pore size at around 200 nm, as shown in Fig. S2. The corresponding, the thickness of AAO with different reaction times was measured, as shown in Fig. 2(o). The film thickness was positively correlated with the reaction time. Thickness was analogous with reaction time and reached 1.5 ± 0.3 μm at 10 s and 8.5 ± 0.9 μm within 60 s. Therefore, nanopore structures with different aspect ratios can be obtained by controlling the thickness of the AAO through controlling the reaction time.

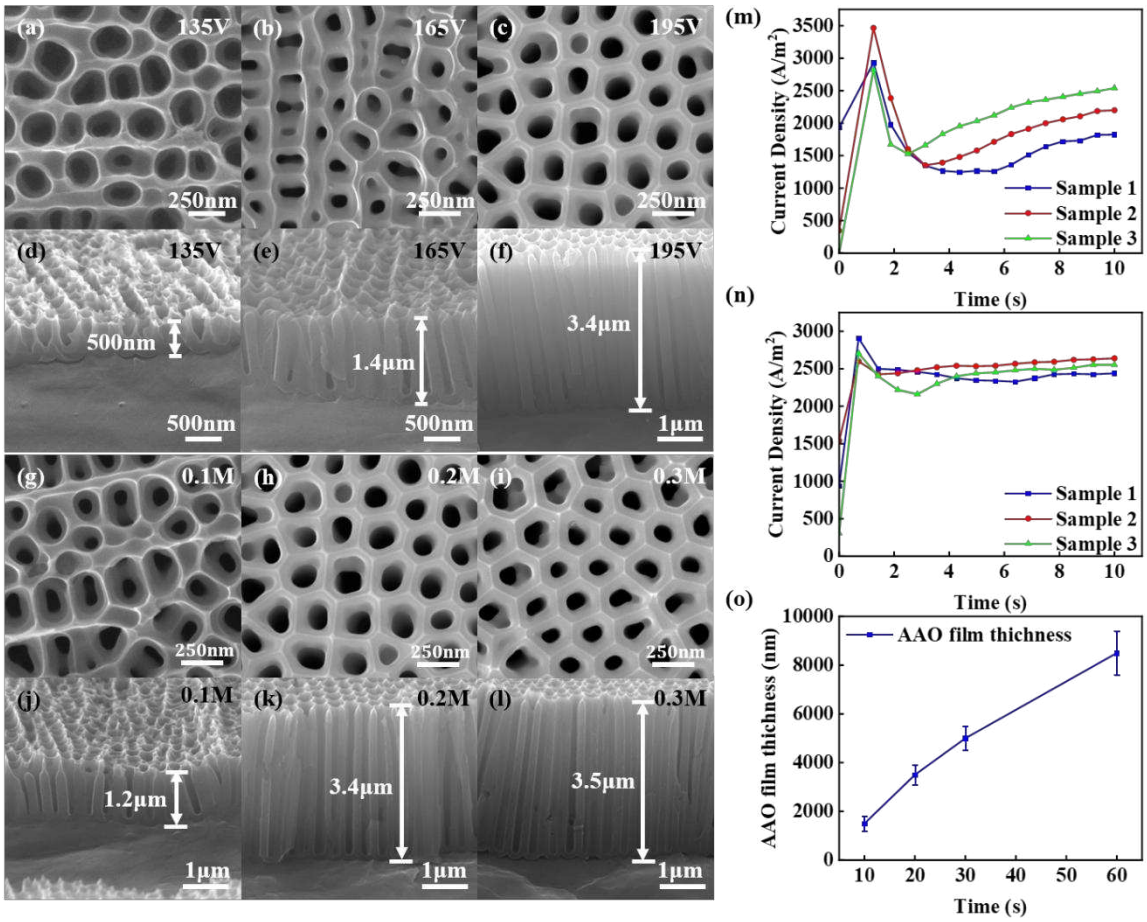

Figure 2. Surface (a-c) and cross-sectional (d-f) SEM images of AAO template at 135V, 165V and 195V respectively; Surface (g-i) and cross-sectional (j-l) SEM images of AAO template at 0.1M, 0.2M and 0.3M of phosphoric acid concentrations respectively; (m) Current density curve during the primary anodic oxidation; (n) Current density curve during the secondary anodic oxidation; (o) Relationship between reaction time and AAO film thickness.

3.2. Nanopillars with different aspect ratios by injection molding

The high aspect ratio structure at the nanoscale is prone to tensile fracture and deformation defects in injection molding. To investigate the influence of different process parameters on the quality of injection molding of high aspect ratio PC nanopillars, single-factor experiments were conducted on different process parameters, as shown in Fig.S3. More detailed information on the regulation during the injection molding process can be seen from the supplementary information and Fig. S4. In terms of the replication quality of nanopillars, increasing the mold temperature was the most effective method. The process parameters for subsequent cell culture substrates were as follows: melt temperature of 290 ℃, cooling time of 150 s, and mold temperature of 140 ℃, holding time of 1 s and holding pressure of 20 MPa.

During the demolding process, the nanopillars were stretched due to the demolding force

generated by the adhesion between the polymer and the mold insert, resulting in the higher nanopillars than the depth of the nanopores. The smallest part of the diameter appeared in the middle of the nanopillars due to the stretching. When the mold temperature was lower than the thermal deformation temperature of PC at 124 ℃, the polymer could not enter the nanopores for filling, as shown in Fig. 3(a-c). As the mold temperature increased, more polymer melts were filled into the nanopores. At the same time, the greater deformation caused by stretching were also observed, as shown in Fig. 3(d-f) and Fig. 3(n-o).

By optimizing the process parameters of injection molding, the fabrication of nanopillars with different aspect ratios can be achieved. Based on this, four groups of nanopillar structures with the same diameter of 200 nm but different aspect ratios were selected for cell culture. The aspect ratios of the nanopillars on the culture substrates were 0, 2.5, 6.5, and 10, encoded as (g) PC, (h) PC-2.5, (i) PC-6.5, and (j) PC-10, as shown in Fig. 3(g-j). The increase of the aspect ratio appears to be influencing the transparency of the samples in a reverse analogous function. In Fig. 3(k-m), the height and aspect ratio of the three components increased linearly, which was consistent with the regulation of the aspect ratio of nanopores in this study, as shown in Fig. 3(p). This provides a good basis for exploring the effects of different aspect ratios of nanopillars on stem cell proliferation and differentiation.

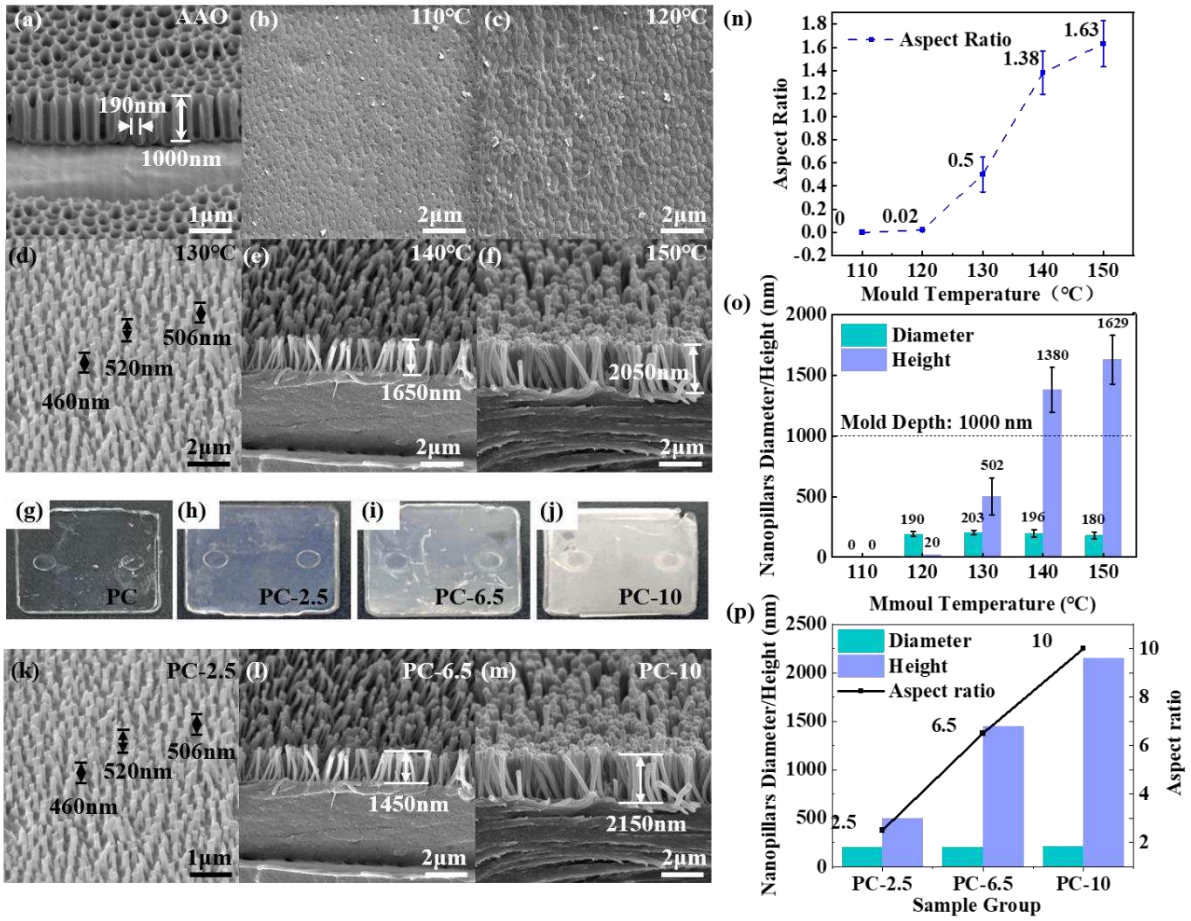

Figure 3. SEM images of AAO mold insert (a) and injection-molded nanopillars at 110 °C (b), 120°C (c), 130°C (d), 140°C (e), 150°C (f) mold temperatures; Nanopillar incubation substrates with aspect ratios of 0 (g), 2.5 (h), 6.5 (i) and 10 (j) ; SEM images of PC substrates with of aspect ratios of 2.5 (k), 6.5 (l) and 10 (m); (n) Tensile ratio variation of nanopillars relative to 1000nm deep nanopores with different mold temperatures; (o) Height and diameter of nanopillars with different mold temperatures, (p) Aspect ratio statistics of nanopillars.

3.3. Adhesion and Proliferation of BMSCs on PC Nanopillar

To detect the proliferation and cellular activity of BMSCs on nanopillars with different aspect ratios, live/dead cell staining was performed on cells cultured on the structure surface. Living cells were stained green with calcein, and the dead cells were stained red with propidium iodide, as shown in Fig. 4. The staining was performed after 24 h and 48 h of culture, and there was no significant cell death in all four groups, indicating normal proliferation activity. BMSCs on the surface of the substrate with nanopillars shown a more circular morphology after 24 h. This was because the cell density was low in the early stage of culture, and the surface nanopillars inhibited cell migration and adhesion, rather than leading to cell death. Regardless

of the reason, this result clearly demonstrates the effect of the presence of nanopillars on the culture surface to the morphology of BMSCs. Evidently, the cells can still adhere and proliferate on the culture surface without any signs of becoming apoptotic, which can be considered as an early sign of biocompatibility.

The CCK-8 test directly reflects on the proportion of live cells in the sample. This experiment employed unmodified commercial culture dishes as the control sample, where cell status was detected at 1, 3 and 6 days, respectively, and the results were shown in Fig. S5. From the first day to the third day, the proliferation trend of BMSCs was not significant. Initially, the activity of BMSCs that were cultured on nanopillars was slightly lower than that of the control, indicating that the PC nanopillars had inhibitory effects on the proliferation of BMSCs. From the third to the sixth day, the proliferation activity of BMSCs in all groups significantly increased, with doubled the number of cells compared to before. It is important to note that, the proliferation activity of the PC-2.5 group was lower than that of the other groups. The proliferation of BMSCs was influenced by the mechanical properties of the surface of nanopillars. Due to the higher substrate surface stiffness in the PC-2.5 group, there was a greater resistance to cell growth. However, as the aspect ratio increases, the substrate surface stiffness becomes lower and the resistance to BMSCs decreases. In addition, previous studies have shown that changes in cell morphology and proliferation were closely related to cell differentiation[45]. Therefore, it can be preliminarily inferred that nanopillars with different aspect ratios have varying degrees of effects on the differentiation of BMSCs. Further testing of cell cytoskeleton and differentiation-related indicators will be conducted.

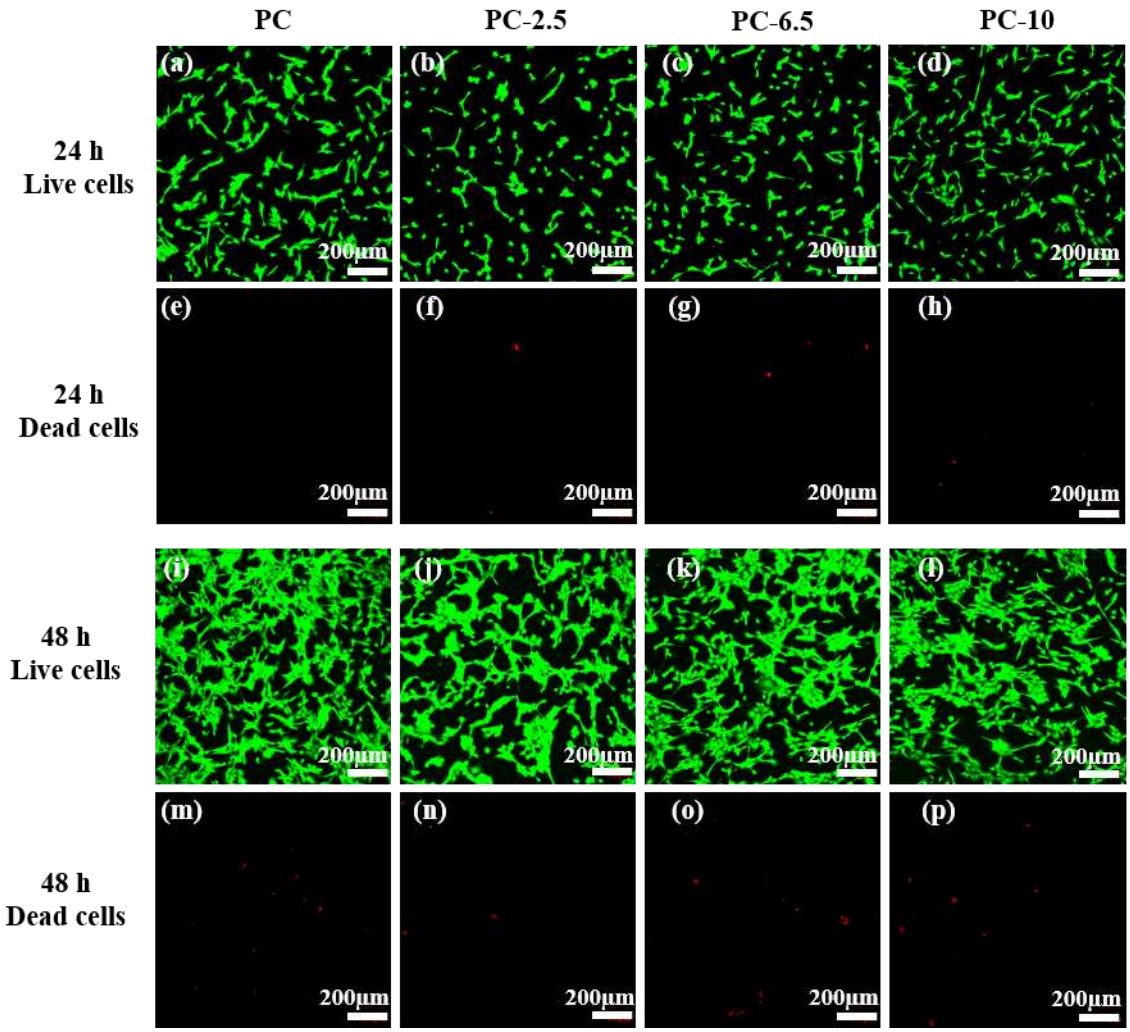

Figure 4. Fluorescence microscopy images of live/dead cell staining of BMSCs cultured on nanopillar substrates with different aspect ratios for 24 h and 48 h. Living cells were stained with Calcein-AM and showed green fluorescence, while dead cells were stained with PI (Propidium iodide) and showed red fluorescence.

3.4. BMSCs differentiation by PC nanopillars

The fluorescence microscopy images of F-actin, Vinculin, and cell nucleus staining of BMSCs cultured for 48 h were shown in Fig. 5. The experiment showed that the proliferation of BMSCs was significantly slowed down, the cell morphology changed, and the adhesion proteins of the cells were clearly distinguished. Based on the results of F-actin staining, the cell morphology of MBSCs on different culture can be compared. In Fig. 5(a), (e), (i) and (m), the cell morphology in the PC group tended to be more polygonal and the cell morphologies in PC-2.5, PC-6.5, and PC-10 groups were slender. Our hypothesis is that it may be due to the decrease in surface stiffness of the culture caused by the increase in the aspect ratio of the

nanopillars. The staining results of Vinculin showed that the fluorescence intensity of PC-6.5 and PC-10 groups was much higher than that of PC and PC-2.5 groups, as shown in Fig. 5(b), (f), (g) and (n), indicating that high-aspect-ratio nanopillars enhanced the adhesion and mechanosensing of BMSCs, which may be associated with subsequent osteogenic differentiation[47,48]. In nuclear staining, it was found that the density of cells with nanopillars was lower than that of the PC group, as shown in Fig. 5(c), (g), (k) and (o). The weakening of cell proliferation may also be related to cell differentiation. Therefore, the decrease in cell density may indicate that BMSCs have a certain differentiation trend on substrates with nanopillar structures.

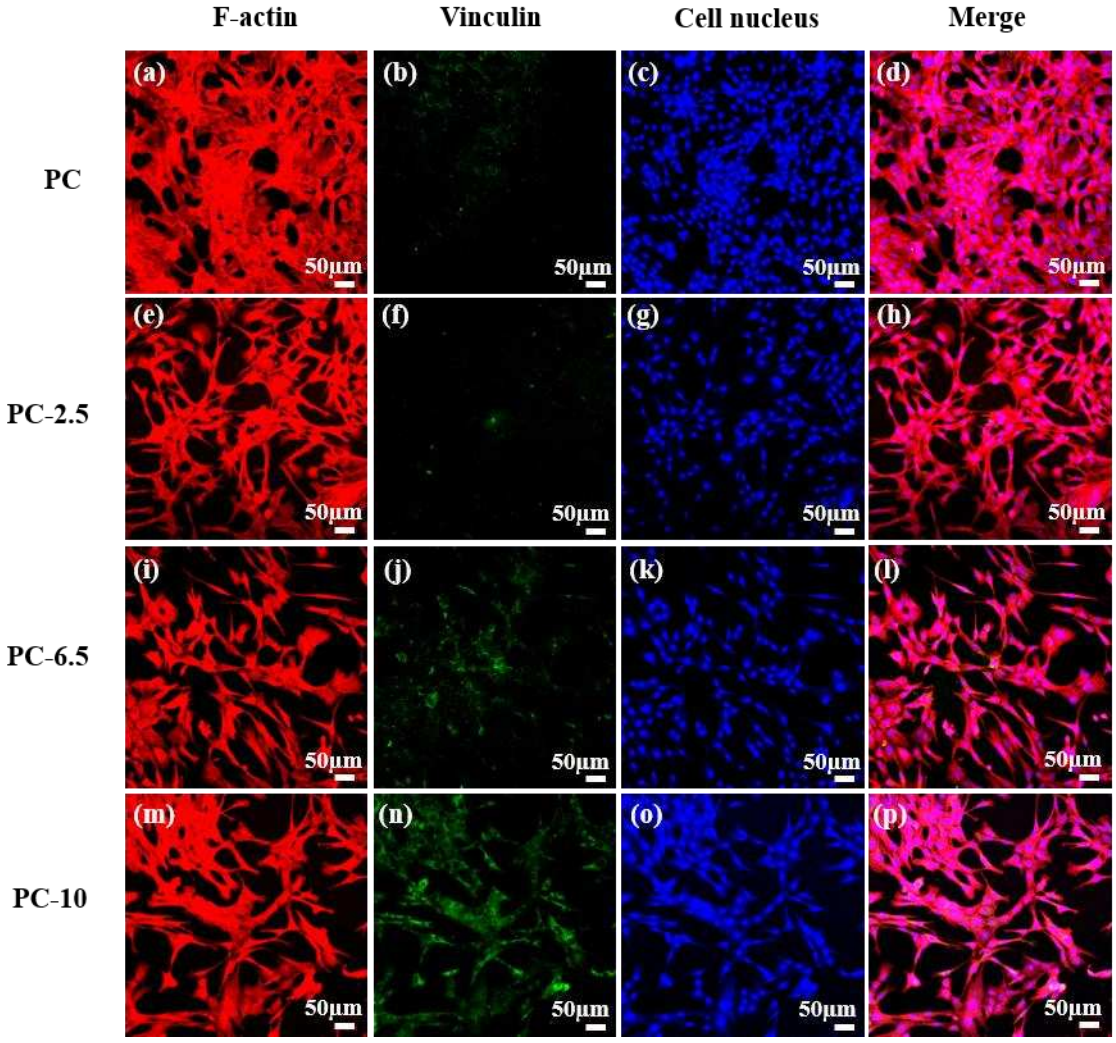

Figure 5. Fluorescence staining microscopy images of BMSCs after 48 h culture on PC (a-d), PC-2.5 (e-h), PC-6.5 (i-l), and PC-10 (m-p) substrates, respectively. F-actin was stained with red fluorescence by Rhodamine Phalloidin; Vinculin was stained with green fluorescence by Goal Anti Rabbit IgG (H+L) FITC conjugated staining; The cell nucleus was stained blue by

DAPI solution.

The ALP is also considered as an initial marker of osteoblast phenotype and differentiation, as the ALP is a by-product of osteoblast activity. In order to characterize the effect of inducing differentiation, a control group and a model group were utilized. Based on the ALP staining results, as well as the quantitative detection of ALP activity in Fig. 6(b), it was found that the control group did not show significant ALP activity, indicating that BMSCs did not undergo osteogenic differentiation. However, in the model group, BMSCs had normal osteogenic differentiation due to the action of osteogenic medium and inducing agents, and ALP activity gradually increased with time. Due to the absence of nanostructures on the substrate surface of the PC group, it was impossible to induce osteogenic differentiation of BMSCs through external stimulation, therefore ALP was not stained on the PC surface. However, a certain staining effect was observed in the contact area between the PC substrate and the 6-well plate substrate, as the changes in the two materials affected the state of the cells. Focusing solely on the groups with nanopillars, the quantitative analysis showed that the ALP activity of the PC-2.5, PC-6.5, and PC-10 groups was higher than that of the model group, proving that the nanopillars can effectively induce the differentiation, analogously with the aspect ratio of nanopillars.

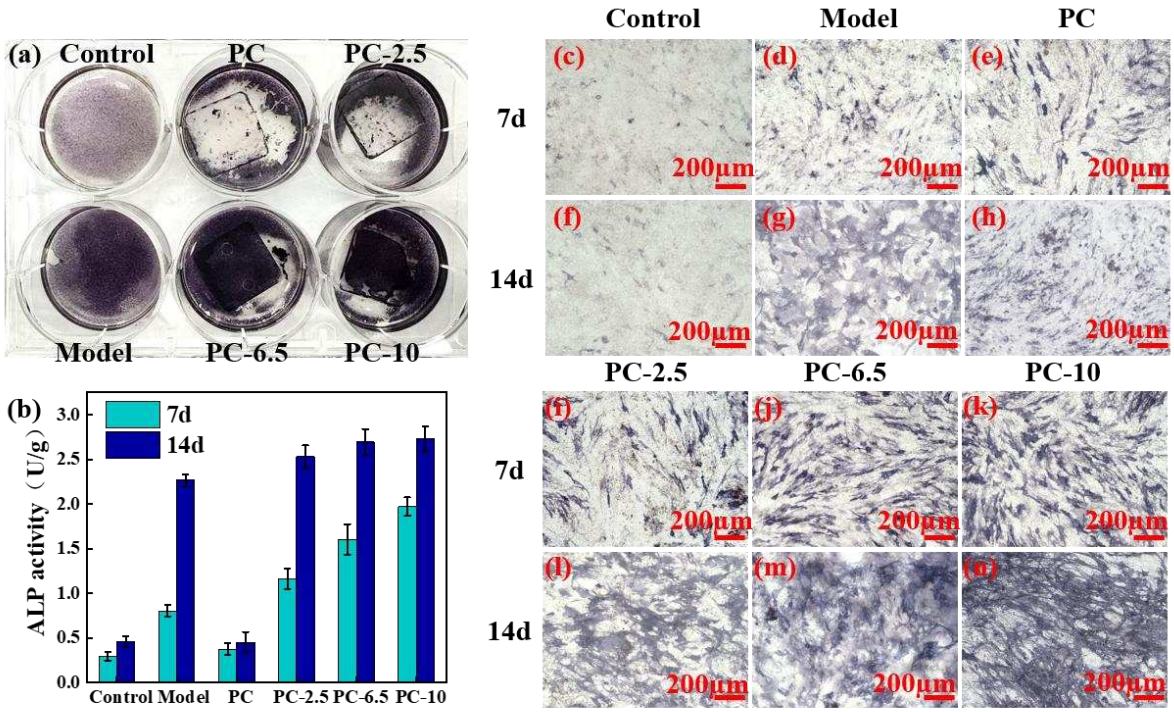

Figure 6. (a) The optical images of ALP staining results; (b) ALP activity quantitative by absorbance detection of BMSCs cultured on different substrates for 7 and 14 days; ALP staining microscopy images of BMSCs cultured for 7 or 14 days in the control group (c), (f), model group (d), (g), PC group (e), (h), PC-2.5 group (i), (l), PC-6.5 group (j), (m), and PC-10 groups (k), (n).

The calcium nodule is one of the late markers of osteogenic differentiation, mainly formed by hydroxyapatite deposition. The ARS staining was performed on the day 21 of BMSCs culture. As shown in Fig. 7(a), the BMSCs in the model group produced a large number of calcified nodules under the action of chemical induction reagents, indicating the osteogenic differentiation of BMSCs. The calcium nodules in the control group, PC group, and PC-2.5 group were relatively few, while the staining effect of the calcium nodules in the PC-6.5 group and PC-10 group was significant, comparable to the staining effect of the model group, as shown in Fig. 7(b). By comparing the ARS staining of BMSCs on PC nanopillars with different aspect ratios, it was found that the control group had almost no calcium nodules, and the PC group had a small amount, while the ARS staining effects were more pronounced in the PC-2.5, PC-6.5, and PC-10 groups, indicating that the nanopillars structure had an inducing effect on the osteogenic differentiation, as shown in Fig. 7(e-g). In addition, the quantitative results of ARS staining presented in Fig. 7(h) indicated that the PC-10 group showed the most significant staining effect, even significantly higher than the model group, indicating that as the aspect ratio of the nanopillars increased, the surface stiffness of the substrate decreased, and nanopillars had a stronger osteogenic differentiation induction effect on BMSCs.

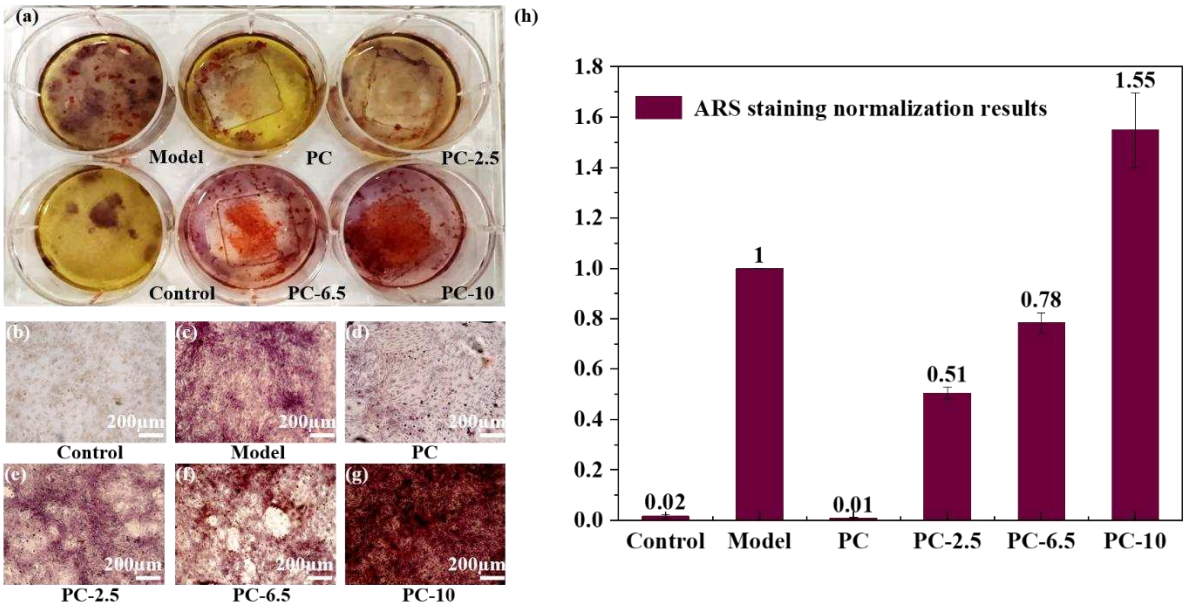

Figure 7. (a)The optical images of calcium nodules stained with ARS after culturing BMSCs on different substrates for 21 days; Calcium nodules staining microscopy images of BMSCs cultured for 21 days in the control group (b), model group (c), PC group (d), PC-2.5 group (e), PC-6.5 group (f), and PC-10 groups (g); (h) Normalized results of ARS staining based on the model group.

Combining the experimental results with the previously reported conclusion that nanopillar stiffness regulates osteogenic differentiation, the stiffness of the nanopillars fabricated in this study was analyzed and calculated. Based on the force analysis model at the free end of the cantilever beam shown in Fig.S6, the stiffness of nanopillars was calculated in the supplementary materials. The Formula (S-5) demonstrates that nanopillar stiffness is directly correlated with the aspect ratio. The analytical results reveal that, under the condition of a constant diameter, nanopillars with a larger aspect ratio exhibit lower stiffness. Moreover, nanopillars with lower stiffness exert a superior promoting effect on the osteogenic differentiation of BMSCs.

Considering the potential adverse effects of 21-day cell culture on PC nanopillars, the PC-10 group with the lowest stiffness was selected to observe the surface morphology of nanopillars before and after cell culture. After 21 days of culture, the cells on the PC nanopillars were thoroughly removed, and oxygen plasma treatment was applied to clean the sample surface. The morphological characteristics of nanopillars were characterized by SEM, as shown

in Fig.S7. The nanopillar structure and morphology remained intact without obvious fracture after long-term cell culture, and their structure, morphology and arrangement were highly consistent with those before cell culture. These results demonstrate that the fabrication method developed in this study is robust and applicable to long-term induction culture of stem cells.

Taken together, it can be concluded that the nanopillars could provide constant external stimulation to adherent BMSCs, which affect the morphology of the cytoskeleton, the production of Vinculin, and the osteogenic differentiation of BMSCs. Nanopillars with different aspect ratios exhibit distinct bending stiffness. As the aspect ratio increases, the nanopillars become softer with reduced stiffness. Based on the mechanical differences between hard and soft nanopillars[30,31,39], mechanical stimulation is transduced through YAP and other related pathways[45,47], thereby driving varying degrees of osteogenic differentiation in BMSCs. Based on the experimental results, the nanopillar structures with different aspect ratios have different induction effects on BMSCs, that the larger the aspect ratio, the stronger the induction effect on BMSCs.

4. Conclusions

In this work, a process chain combining self-assembled mold inserts and injection molding was proposed to fabricate nanopillar structures with different aspect ratios as the substrates for cell culture. The optimal parameters affecting the anodic oxidation process for the mold inserts and the injection molding process for the nanopillar substrates were investigated. Nanopore structures with different aspect ratios can be obtained by controlling the thickness of the AAO through controlling the reaction time. In the injection molding process, increasing the mold temperature was the most effective method to improve the height of nanostructures considering the replication quality, and nanopillars with aspect ratios of 2.5, 6.5, and 10 were obtained. The injection-molded nanopillars were then applied to the culture and differentiation experiments of bone marrow mesenchymal stem cells. The results in evaluation indicators such as the ALP activity and calcium nodules indicated that as the aspect ratio of the nanopillar increases, their ability to induce osteogenic differentiation was enhanced, and the degree of differentiation induced by the nanopillars was greater than that of the model group induced by osteogenic inducers, with the PC-10 group showing the most significant differentiation induction effect.

Our research can be applied to the manufacturing of a wider range of polymer materials and structures, enriching the methods for regulating stem cell fate in biomaterials and providing new research directions for tissue regeneration in different organs.

Declaration of Competing Interest

The authors declare that they have no known competing financial interests or personal relationships that could have appeared to influence the work reported in this paper.

Acknowledgement

This research was supported by the National Natural Science Foundation of China (Key International Joint Research Program, No: 51920105008), Natural Science Foundation of Changsha City, China (No: kq2402212), the project of State Key Laboratory of Precision Manufacturing for Extreme Service Performance, Central South University (No: ZZYJKT2024-15), and Fundamental Research Funds for the Central Universities of Central South University (No: 2024ZZTS0790).

Data Availability

All data generated or analyzed during this study are included in this submitted article and its supplementary information file.

References

[1] M. Aleksanyan, A. Sayunts, G. Shahkhatuni, Z. Simonyan, D. Kananov, E. Khachaturyan, R. Papovyan, A. Michalcová, D. Kopecký, SnO2/MWCNTs Nanostructured Material for High-Performance Acetone and Ethanol Gas Sensors, ACS Omega 10 (2025) 7283–7294. https://doi.org/10.1021/acsomega.4c10981.

[2] A. Ashok, T.K. Nguyen, M. Barton, M. Leitch, M.K. Masud, H. Park, T.A. Truong, Y.V. Kaneti, H.T. Ta, X. Li, K. Liang, T.N. Do, C.H. Wang, N.T. Nguyen, Y. Yamauchi, H.P. Phan, Flexible Nanoarchitectonics for Biosensing and Physiological Monitoring Applications, Small 19 (2023). https://doi.org/10.1002/smll.202204946.

[3] P. Moitra, X. Xu, R. Maruthiyodan Veetil, X. Liang, T.W.W. Mass, A.I. Kuznetsov, R. Paniagua-Domínguez, Electrically Tunable Reflective Metasurfaces with Continuous and Full-Phase Modulation for High-Efficiency Wavefront Control at Visible Frequencies, ACS Nano 17 (2023) 16952–16959. https://doi.org/10.1021/acsnano.3c04071.

[4] G. Cai, Y. Li, Y. Zhang, X. Jiang, Y. Chen, G. Qu, X. Zhang, S. Xiao, J. Han, S. Yu, Y. Kivshar, Q. Song, Compact angle-resolved metasurface spectrometer, Nat. Mater. 23 (2024) 71–78. https://doi.org/10.1038/s41563-023-01710-1.

[5] J. Song, Y. Hou, P. Sudersan, C.W.E. Lam, D. Poulikakos, H.J. Butt, K.L. Yeung, Inhibition of condensation-induced droplet wetting by nano-hierarchical surfaces, Chemical Engineering Journal

460 (2023). https://doi.org/10.1016/j.cej.2023.141761.

[6] S. Wang, Z. Liu, L. Wang, J. Xu, R. Mo, Y. Jiang, C. Wen, Z. Zhang, L. Ren, Superhydrophobic Mechano-Bactericidal Surface with Photodynamic Antibacterial Capability, ACS Applied Materials and Interfaces 15 (2023) 723–735. https://doi.org/10.1021/acsami.2c21310.

[7] Z. Zhang, R. Xu, Y. Yang, C. Liang, X. Yu, Y. Liu, T. Wang, Y. Yu, F. Deng, Micro/nano-textured hierarchical titanium topography promotes exosome biogenesis and secretion to improve osseointegration, J. Nanobiotechnology 19 (2021). https://doi.org/10.1186/s12951-021-00826-3.

[8] L.T. Rao, A. Raz, F. Patolsky, Biomarker analysis from complex biofluids by an on-chip chemically modified light-controlled vertical nanopillar array device, Nat. Protoc. 20 (2025) 2286–2318. https://doi.org/10.1038/s41596-024-01124-6.

[9] C.M. Kolf, E. Cho, R.S. Tuan, Mesenchymal stromal cells. Biology of adult mesenchymal stem cells: Regulation of niche, self-renewal and differentiation, Arthritis Res. Ther. 9 (2007). https://doi.org/10.1186/ar2116.

[10] L. Song, N.E. Webb, Y. Song, R.S. Tuan, Identification and Functional Analysis of Candidate Genes Regulating Mesenchymal Stem Cell Self-Renewal and Multipotency, Stem Cells 24 (2006) 1707–1718. https://doi.org/10.1634/stemcells.2005-0604.

[11] Y. Nishimura, T. Aida, Y. Taguchi, Advances in tissue engineering technology for kidney regeneration and construction, Journal of Artificial Organs 25 (2022) 191–194. https://doi.org/10.1007/s10047-022-01315-6.

[12] X. Wu, J. Su, J. Wei, N. Jiang, X. Ge, Recent Advances in Three-Dimensional Stem Cell Culture Systems and Applications, Stem Cells Int. 2021 (2021). https://doi.org/10.1155/2021/9477332.

[13] L. Zhang, W. Liao, S. Chen, Y. Chen, P. Cheng, X. Lu, Y. Ma, Towards a New 3Rs Era in the construction of 3D cell culture models simulating tumor microenvironment, Front. Oncol. 13 (2023). https://doi.org/10.3389/fonc.2023.1146477.

[14] T. Trantidou, C.M. Terracciano, D. Kontziampasis, E.J. Humphrey, T. Prodromakis, Biorealistic cardiac cell culture platforms with integrated monitoring of extracellular action potentials, Sci. Rep. 5 (2015). https://doi.org/10.1038/srep11067.

[15] L. Zheng, Z. Zhuang, Y. Li, T. Shi, K. Fu, W. Yan, L. Zhang, P. Wang, L. Li, Q. Jiang, Bone targeting antioxidative nano-iron oxide for treating postmenopausal osteoporosis, Bioact. Mater. 14 (2022) 250–261. https://doi.org/10.1016/j.bioactmat.2021.11.012.

[16] Y. Zhang, P. Wang, H. Mao, Y. Zhang, L. Zheng, P. Yu, Z. Guo, L. Li, Q. Jiang, PEGylated gold nanoparticles promote osteogenic differentiation in in vitro and in vivo systems, Mater. Des. 197 (2021). https://doi.org/10.1016/j.matdes.2020.109231.

[17] G. Tullii, F. Giona, F. Lodola, S. Bonfadini, C. Bossio, S. Varo, A. Desii, L. Criante, C. Sala, M. Pasini, C. Verpelli, F. Galeotti, M.R. Antognazza, High-Aspect-Ratio Semiconducting Polymer Pillars for 3D Cell Cultures, ACS Appl. Mater. Interfaces 11 (2019) 28125–28137. https://doi.org/10.1021/acsami.9b08822.

[18] A.L.R. Rangel, C. Falentin-Daudré, B.N.A. da Silva Pimentel, C.E. Vergani, V. Migonney, A.P.R. Alves Claro, Nanostructured titanium alloy surfaces for enhanced osteoblast response: A combination of morphology and chemistry, Surf. Coat. Technol. 383 (2020). https://doi.org/10.1016/j.surfcoat.2019.125226.

[19] Y. Zhang, S. Cui, S. Cao, L. Yang, G. Qin, E. Zhang, To improve the angiogenesis of endothelial cells on Ti-Cu alloy by the synergistic effects of Cu ions release and surface nanostructure, Surf. Coat. Technol. 433 (2022). https://doi.org/10.1016/j.surfcoat.2022.128116.

[20] M. Kitsara, D. Kontziampasis, O. Agbulut, Y. Chen, Heart on a chip: Micro-nanofabrication and microfluidics steering the future of cardiac tissue engineering, Microelectron. Eng. 203–204 (2019) 44–62. https://doi.org/10.1016/j.mee.2018.11.001.

[21] M. Kitsara, O. Agbulut, D. Kontziampasis, Y. Chen, P. Menasché, Fibers for hearts: A critical review on electrospinning for cardiac tissue engineering, Acta Biomater. 48 (2017) 20–40. https://doi.org/10.1016/j.actbio.2016.11.014.

[22] Y. Osada, T. Yanagishita, Effects of anodization conditions of stainless steel on the formation of ordered nanoporous structures with high aspect ratios, Nanotechnology 34 (2023). https://doi.org/10.1088/1361-6528/acef2a.

[23] M. Kitsara, D. Kontziampasis, E. Bolomiti, A. Simon, P. Dimitrakis, A. Miche, G. Kokkoris, V. Humblot, O. Agbulut, Surfaces for hearts: Establishing the optimum plasma surface engineering methodology on polystyrene for cardiac cell engineering, Appl. Surf. Sci. 620 (2023). https://doi.org/10.1016/j.apsusc.2023.156822.

[24] J. Zajadacz, P. Lorenz, M. Ehrhardt, K. Zimmer, Development platform for UV-NIL processes using polymer masters produced by laser ablation and photolithography, Nanotechnology and Precision Engineering 8 (2025). https://doi.org/10.1063/10.0034395.

[25] X. Xue, X. Tang, C. Hu, J. Sun, X. Li, S. Yang, S. Kerman, S. Xie, X. Xu, R. Ji, C. Chen, High-uniformity, low-cost, ultra-dense arrays of Au-capped plastic nanopillars fabricated via nanoimprint lithography as reliable SERS substrates, Spectrochim. Acta A Mol. Biomol. Spectrosc. 335 (2025). https://doi.org/10.1016/j.saa.2025.125989.

[26] D. Masato, M. Sorgato, G. Lucchetta, Analysis of the influence of part thickness on the replication of micro-structured surfaces by injection molding, Mater. Des. 95 (2016) 219–224. https://doi.org/10.1016/j.matdes.2016.01.115.

[27] J.M. Stormonth-Darling, N. Gadegaard, Injection moulding difficult nanopatterns with hybrid polymer inlays, Macromol. Mater. Eng. 297 (2012) 1075–1080. https://doi.org/10.1002/mame.201100397.

[28] G. Lucchetta, M. Sorgato, S. Carmignato, E. Savio, Investigating the technological limits of micro-injection molding in replicating high aspect ratio micro-structured surfaces, CIRP Ann. Manuf. Technol. 63 (2014) 521–524. https://doi.org/10.1016/j.cirp.2014.03.049.

[29] T. Tanaka, M. Hirose, N. Kotobuki, H. Ohgushi, T. Furuzono, J. Sato, Nano-scaled hydroxyapatite/silk fibroin sheets support osteogenic differentiation of rat bone marrow mesenchymal cells, Materials Science and Engineering C 27 (2007) 817–823. https://doi.org/10.1016/j.msec.2006.09.019.

[30] M. Sorgato, E. Guidi, M.T. Conconi, G. Lucchetta, Surface nanostructuring of bioresorbable implants to induce osteogenic differentiation of human mesenchymal stromal cells, CIRP Annals 70 (2021) 463–466. https://doi.org/10.1016/j.cirp.2021.04.011.

[31] C.H. Rasmussen, P.M. Reynolds, D.R. Petersen, M. Hansson, R.M. McMeeking, M. Dufva, N. Gadegaard, Enhanced Differentiation of Human Embryonic Stem Cells Toward Definitive Endoderm on Ultrahigh Aspect Ratio Nanopillars, Adv. Funct. Mater. 26 (2016) 815–823. https://doi.org/10.1002/adfm.201504204.

[32] K. Li, L. Lv, D. Shao, Y. Xie, Y. Cao, X. Zheng, Engineering Nanopatterned Structures to Orchestrate Macrophage Phenotype by Cell Shape, J. Funct. Biomater. 13 (2022). https://doi.org/10.3390/jfb13010031.

[33] T. Risom, D.R. Glass, I. Averbukh, C.C. Liu, A. Baranski, A. Kagel, E.F. McCaffrey, N.F. Greenwald,

B. Rivero-Gutiérrez, S.H. Strand, S. Varma, A. Kong, L. Keren, S. Srivastava, C. Zhu, Z. Khair, D.J. Veis, K. Deschryver, S. Vennam, C. Maley, E.S. Hwang, J.R. Marks, S.C. Bendall, G.A. Colditz, R.B. West, M. Angelo, Transition to invasive breast cancer is associated with progressive changes in the structure and composition of tumor stroma, Cell 185 (2022) 299-310.e18. https://doi.org/10.1016/j.cell.2021.12.023.

[34] J. Chato-Astrain, F. Campos, O. Roda, E. Miralles, D. Durand-Herrera, J.A. Sáez-Moreno, S. García-García, M. Alaminos, A. Campos, V. Carriel, In vivo evaluation of nanostructured fibrin-agarose hydrogels with mesenchymal stem cells for peripheral nerve repair, Front. Cell. Neurosci. 12 (2018). https://doi.org/10.3389/fncel.2018.00501.

[35] P. Joanne, M. Kitsara, S.E. Boitard, H. Naemetalla, V. Vanneaux, M. Pernot, J. Larghero, P. Forest, Y. Chen, P. Menasché, O. Agbulut, Nanofibrous clinical-grade collagen scaffolds seeded with human cardiomyocytes induces cardiac remodeling in dilated cardiomyopathy, Biomaterials 80 (2016) 157–168. https://doi.org/10.1016/j.biomaterials.2015.11.035.

[36] M. Kitsara, A. Blanquer, G. Murillo, V. Humblot, S. De Bragança Vieira, C. Nogués, E. Ibáñez, J. Esteve, L. Barrios, Permanently hydrophilic, piezoelectric PVDF nanofibrous scaffolds promoting unaided electromechanical stimulation on osteoblasts, Nanoscale 11 (2019) 8906–8917. https://doi.org/10.1039/c8nr10384d.

[37] S. Hashimoto, M. Yasunaga, M. Hirose, M. Kakehata, H. Yashiro, A. Yamazaki, A. Ito, Cell attachment area of rat mesenchymal stem cells correlates with their osteogenic differentiation level on substrates without osteoconductive property, Biochem. Biophys. Res. Commun. 525 (2020) 1081–1086. https://doi.org/10.1016/j.bbrc.2020.03.013.

[38] Y. Yang, S. Wu, R. Qu, C. Wang, J. Wang, A.U. Khan, Y. Pan, W. Liu, J. Zhu, M.A. Khan, C. Xu, J. Dai, J. Ouyang, Mechanical sensor PDLIM5 promotes the osteogenesis of human adipose-derived stem cells through microfilament alterations, Genes Dis. 11 (2024). https://doi.org/10.1016/j.gendis.2023.06.001.

[39] L. Papadimitriou, A. Karagiannaki, E. Stratakis, A. Ranella, Substrate topography affects PC12 cell differentiation through mechanotransduction mechanisms, Mechanobiology in Medicine 2 (2024). https://doi.org/10.1016/j.mbm.2024.100039.

[40] Y. Peng, R. Qu, Y. Yang, T. Fan, B. Sun, A.U. Khan, S. Wu, W. Liu, J. Zhu, J. Chen, X. Li, J. Dai, J. Ouyang, Regulation of the integrin αVβ3- actin filaments axis in early osteogenic differentiation of human mesenchymal stem cells under cyclic tensile stress, Cell Communication and Signaling 21 (2023). https://doi.org/10.1186/s12964-022-01027-7.

[41] W. Wei, Y. Liu, X. Yao, R. Hang, Na-Ti-O nanostructured film anodically grown on titanium surface have the potential to improve osteogenesis, Surf. Coat. Technol. 397 (2020). https://doi.org/10.1016/j.surfcoat.2020.125907.

[42] M.P. Lutolf, P.M. Gilbert, H.M. Blau, Designing materials to direct stem-cell fate, Nature 462 (2009) 433–441. https://doi.org/10.1038/nature08602.

[43] W. Liang, C. Zhou, X. Liu, Q. Xie, L. Xia, Q. Li, H. Lin, X. Xiong, H. Zhang, Z. Zheng, J. Zhao, Synthetic Nanopillars for Stimulating Osteoblast Activity and Osteointegration in Bone-Related Disorders, Int. J. Nanomedicine 20 (2025) 2205–2223. https://doi.org/10.2147/IJN.S501963.

[44] E. Zanchetta, E. Guidi, G. Della Giustina, M. Sorgato, M. Krampera, G. Bassi, R. Di Liddo, G. Lucchetta, M.T. Conconi, G. Brusatin, Injection molded polymeric micropatterns for bone regeneration study, ACS Appl. Mater. Interfaces 7 (2015) 7273–7281. https://doi.org/10.1021/acsami.5b00481.

[45] P. Luo, Y. Cheng, Y. Luo, N. Zhang, J. Cao, H. Wang, X. Jiang, Q. Wang, X. Wu, Y. Liu, J. Mao, X. Zhou, J.J. Nie, D. Chen, Hydrogel Enhanced Organoid Multidirectional Differentiation via Yap/Tead4 Mechanotransduction for Accelerated Tissue Regeneration, ACS Appl. Mater. Interfaces 17 (2025) 37601–37616. https://doi.org/10.1021/acsami.5c06161.

[46] S. Zhang, B. Ma, F. Liu, J. Duan, S. Wang, J. Qiu, D. Li, Y. Sang, C. Liu, D. Liu, H. Liu, Polylactic Acid Nanopillar Array-Driven Osteogenic Differentiation of Human Adipose-Derived Stem Cells Determined by Pillar Diameter, Nano Lett. 18 (2018) 2243–2253. https://doi.org/10.1021/acs.nanolett.7b04747.

[47] Y. Zhao, Q. Sun, B. Huo, Focal adhesion regulates osteogenic differentiation of mesenchymal stem cells and osteoblasts, Biomaterials Translational 2 (2021) 312–322. https://doi.org/10.12336/biomatertransl.2021.04.007.

[48] D. Zhang, L. Lai, H. Fu, Q. Fu, M. Chen, 3D-Bioprinted Biomimetic Multilayer Implants Comprising Microfragmented Adipose Extracellular Matrix and Cells Improve Wound Healing in a Murine Model of Full-Thickness Skin Defects, ACS Appl. Mater. Interfaces 15 (2023) 29713–29728. https://doi.org/10.1021/acsami.2c21629.